Proc. Indian Acad. Sci. (Earth Planet. Sci.), Vol. 104, No. 4, December 1995, pp. 693–706.

Seismic moment release along selected major transforms on the Central Indian Ridge, Western Indian Ocean, and its tectonic implications

M RADHA KRISHNA

Marine Geology Division, School of Marine Sciences, Fine Arts Avenue, Cochin University of Science and Technology, Cochin 682 016, India

MS received 4 July 1995; revised 30 October 1995

Abstract. A detailed seismicity map of the Central Indian Ridge for the period 1912–1993 is presented, and the earthquakes pertaining to four major transforms offsetting the ridge are utilized to study the moment release pattern. The scalar moment release for the period 1912–1993, and the summed moment rate tensors for both short period (1977–1993) and long period (1912–1993) bring out a unified picture of moment release pattern.

The fraction of seismic slip calculated based on depths of 100°C and 400°C limiting temperatures suggests that the Marie-Celeste transform requires a slip almost to a depth of 400°C isotherm to account for the observed moment, and the Argo transform requires depth of faulting much above the 400°C isotherm. A very small fraction of slip is accounted seismically for Vema (53%) and 12° 12′S (23%) even to depths of 100°C isotherm, suggesting a very low order of moment release along these transforms.

The horizontal plate velocities and the corresponding strain rates obtained from moment tensor summation of long period data (82 years) give rise to (V_y^y; V_x^y mm.yr^{-1}) of 6·0 and 6·1 along Marie-Celeste, 1·3 and 0·50 along Argo, 0·06 and 0·06 along 12° 12′S, 1·6 and 0·25 along Vema transforms. The corresponding strain rates (ε_y^y; $\varepsilon_x^y \times 10^{-15}$S^{-1}) are 12·7 and 6·8 along Marie-Celeste, 6·9 and 1·4 along Argo, 0·27 and 0·14 along 12° 12′S, 7·3 and 0·58 along Vema transforms.

These results suggest that the strain rates were highest and almost all predicted motion is taken up seismically along the Marie-Celeste transform. The strain rates are lower along Argo transform and the observed moment release require shallower depth of faulting in order to slip to be accounted seismically. The Vema and 12° 12′S transforms are characterized by low strain rates and less than 15 per cent of motion is accommodated seismically within the seismogenic layer. It is proposed that the deficiency of moment release along the Vema and 12° 12′S multiple transform system may be due to most of the plate motion occurring aseismically.

Keywords. Scalar moment release; moment rate tensors; strain rates; major transforms; Central Indian Ridge.

1. Introduction

Transform faults are rigid plate boundaries where the ridge is offset, juxtaposing lithosphere of varying age and thickness against the ridge axis (Wilson 1965). The relative motion is confined to the transform fault between the two spreading ridge segments beyond which the bathymetric expression continues as a fracture zone (Fowler 1990). Earthquakes occurring on the transform faults give an important input in understanding the local plate motions and mid ocean ridge dynamics. While the mechanism of earthquakes and depth of seismogenic faulting gives information on the thermal and mechanical properties of the lithosphere underlying the transform fault (Burr and Solomon 1978; Engeln *et al* 1986), the cumulative moment release and earthquake slip vectors are useful in estimating the direction of local plate motions and

rates of slip along the transform length (Brune 1968; Davies and Brune 1971; Kanamori and Stewart 1976; Engeln *et al* 1986; Wald and Wallace 1986; among others). The seismic slip rates obtained by this method generally correlate well with the full spreading rates estimated from the magnetic anomaly identifications, though notable deviations are observed along some fracture zones like the Eltanin Fracture zone system on the Pacific-Antarctic Ridge (Stewart and Okal 1983).

The topography of the Indian Ocean is dominated by three active mid-ocean ridge systems and these ridges mark the present boundaries of the Indian, African and Antarctic plates. The Central Indian Ridge (CIR), which is a part of these active ridge systems between African and Australian plates, trends in general N–S between 2°N and the triple junction near 25°S in the Central Indian Ocean. In this study, we discuss the seismicity and tectonics of the Central Indian Ridge, through the analysis of the hypocentre trends and seismic slip rates along four major transform faults.

2. Regional geotectonic setting of the Central Indian Ridge

The Central Indian Ridge is a slow spreading ridge trending broadly N–S in an arcuate pattern between 2°N and the Rodriguez Triple Junction at 25°S in the Central Indian Ocean. It is bounded by two aseismic ridges. the Chagos-Laccadive Ridge on the east and the Mascarene plateau on the west (figure 1). Previous geological and geophysical investigations revealed that the ridge consists of a series of en echelon segments offset by numerous NE–SW trending fracture zones (Langseth and Taylor 1967; Fisher *et al* 1967; Banghar and Sykes 1969; Fisher *et al* 1971). The fact that the fracture zones offsetting the ridge do not extend beyond Chagos-Laccadive Ridge eastward or Mascarene plateau westward indicates that these two aseismic ridges existed together as a single ridge until the Eocene and later separated as a consequence of spreading along the Carlsberg Ridge (McKenzie and Sclater 1971; Sclater *et al* 1981).

The various transform faults offsetting the ridge segments and their azimuth have been identified based on the seismicity, bathymetry and magnetic anomalies by Fisher *et al* (1971). Finer aspects of discontinuities of the spreading ridge segments in the southern part of CIR have been studied by Parson *et al* (1993). Magnetic anomalies and NUVEL-1 indicate that the current half spreading rate varies from 1·6 to 2·5 cm/yr between the northern and southern part of the ridge (Fisher *et al* 1971; DeMets *et al* 1990). North of Vema fracture zone at 9°S, the ridge consists of shorter transforms with short ridge segments between them. Tectonics of the CIR is more complicated in the north due to the unusually high seismicity level of Chagos bank within the intraplate deformation zone (Wiens 1985) and the presence of diffuse triple junction just south of the equator, as proposed by Gordon *et al* (1990).

3. Method of analysis

The seismic slip rate for an individual transform segment can be estimated by summing up the seismic moment for all earthquakes on that transform for a given period of time following Brune (1968) and Davies and Brune (1971):

$$V = \frac{\Sigma M_o}{\mu A T}, \tag{1}$$

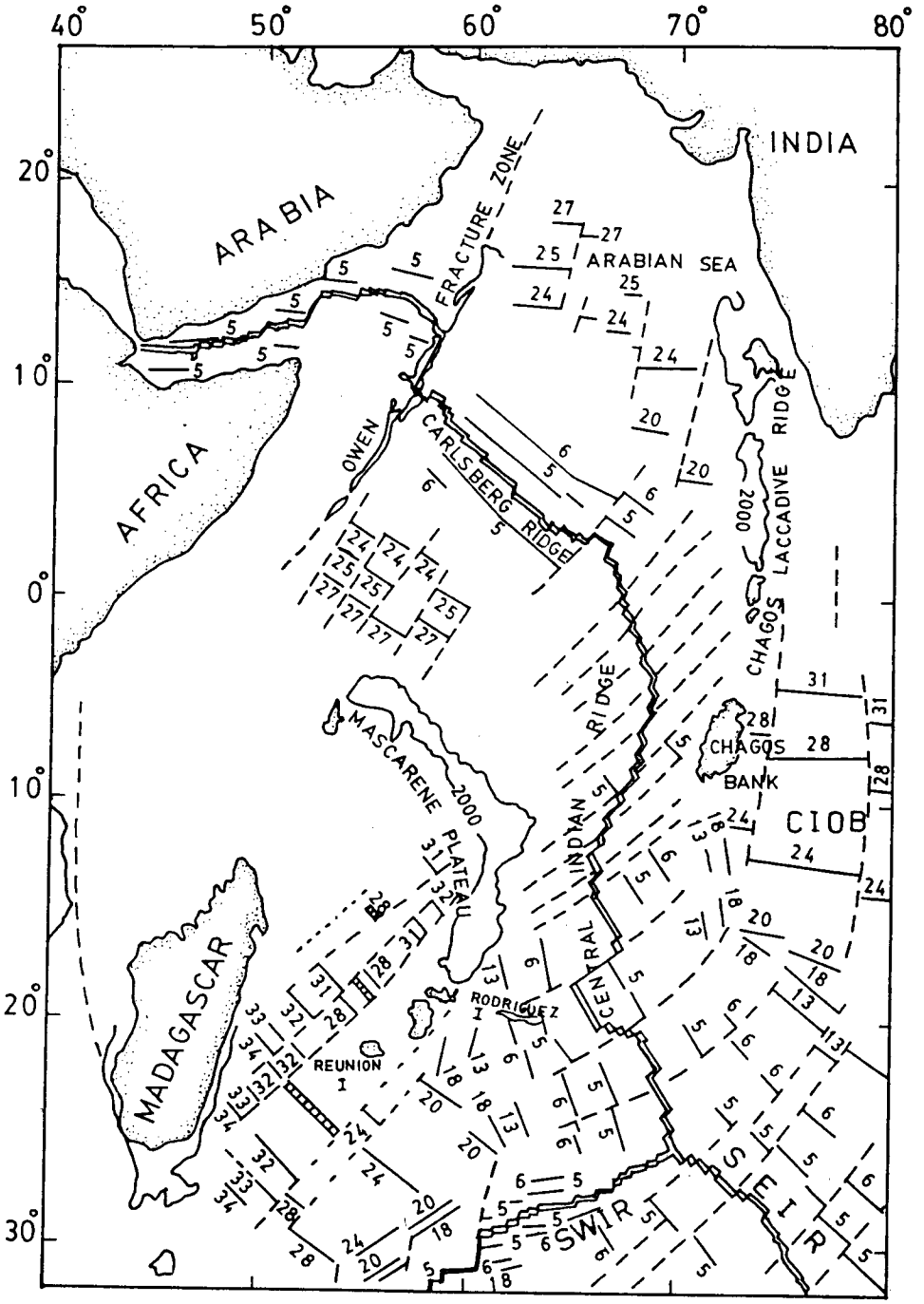

Figure 1. Tectonic sketch map of the western Indian Ocean up to 30°S redrawn after Royer *et al* (1989). Dashed lines are fracture zones, continuous line with number are magnetic anomaly identifications. SWIR – Southwest Indian Ridge, SEIR – Southeast Indian Ridge, CIOB – Central Indian Ocean Basin.

where, V = Average slip rate or full spreading rate, ΣM_o = Cumulative moment release during the period T, μ = Rigidity $3{\cdot}3 \times 10^{11}$ dyn. cm^{-2}, A = Fault area.

This relationship assumes that all slip on the transform to an estimated depth of rupture is accomplished by brittle failure and that the interval of observation is sufficiently long to obtain a representative sample of large earthquakes (Burr and Solomon 1978). This approach has been successfully utilized to estimate slip rates on oceanic transforms (eg. Burr and Solomon 1978; Engeln *et al* 1986). The individual seismic moment tensor elements however can be utilized to calculate the components of plate velocities and the seismic strain rate tensors following the method of Jackson and McKenzie (1988), Ekstrom and England (1989) and Holt *et al* (1991) as briefly mentioned below.

The ijth component of seismic moment tensor, M of an earthquake can be obtained from the scalar moment M_o and the information derived from the fault plane solution

$$M_{ij} = M_o(u_i n_j + u_j n_i), \tag{2}$$

where, $\hat{\mathbf{n}}$ is unit vector normal to the fault-plane, $\hat{\mathbf{u}}$ is unit vector in the direction of slip.

Following Kostrov (1974), the average strain ε_{ij} within a volume v is related to the sum of the moment tensors of all earthquakes (n) within it as:

$$\varepsilon_{ij} = \frac{1}{2\mu V} \sum_{n=1}^{N} M_{ij}^n \tag{3}$$

and the average over time interval T gives the moment rate tensor ($\dot{M}$) and the strain rate tensor ($\dot{\varepsilon}_{ij}$).

If l, a, t are length, width and thickness of the fault zone, the average strain rate can be related to the various components of velocities as:

$$\varepsilon = \frac{1}{2}\begin{bmatrix} 2\frac{V_x^x}{l} & \frac{V_x^y}{a} + \frac{V_y^x}{l} & \frac{V_z^x}{l} + \frac{V_x^z}{t} \\ \frac{V_y^x}{l} + \frac{V_x^y}{a} & 2\frac{V_y^y}{a} & \frac{V_y^z}{a} + \frac{V_z^y}{t} \\ \frac{V_z^x}{l} + \frac{V_x^z}{t} & \frac{V_z^y}{a} + \frac{V_y^z}{t} & 2\frac{V_z^z}{t} \end{bmatrix}. \tag{4}$$

Within each transform zone, if $\mathbf{u}$ is unit vector in the predicted slip direction, V is magnitude of velocity and $\mathbf{n}$ is unit vector normal to the boundary of the transform zone, the matrix $\mathbf{N}$ can be formed as:

$$\mathbf{N} = \mu l t v \begin{bmatrix} 2n_1u_1 & (n_1u_2 + n_2u_1) & 0 \\ (n_1u_2 + n_2u_1) & 2n_2u_2 & 0 \\ 0 & 0 & -2(n_1u_1 + n_2u_2) \end{bmatrix} \tag{5}$$

and the elements N_{11}, N_{22}, N_{12} when compared with corresponding elements M_{11}, M_{22} and M_{12} of the summed moment rate tensor ($\dot{M}$) reveal the fraction of

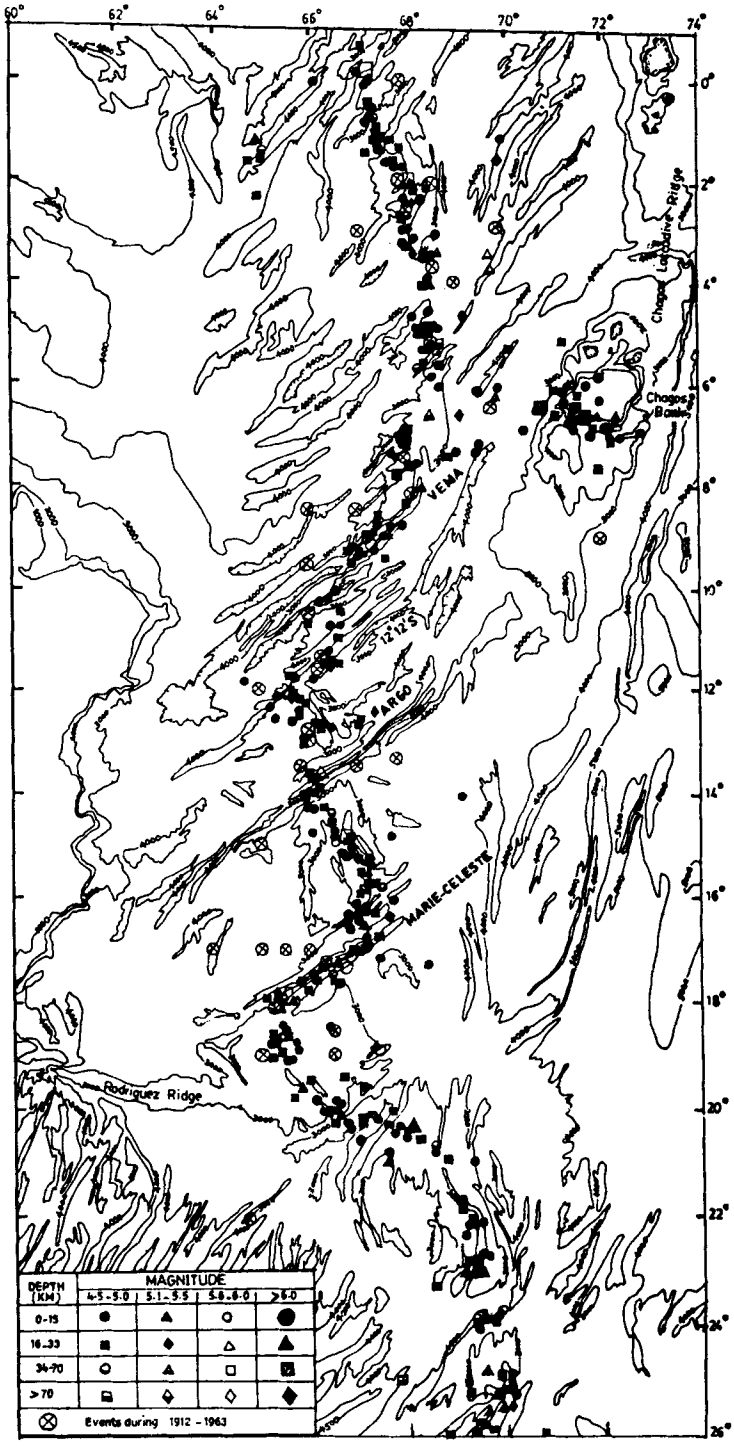

Figure 2. Seismicity of the Central Indian Ridge during the period 1912–1993. Bathymetry is adopted from Fisher *et al* (1971).

Table 1. List of available centroid moment tensor events along the Central Indian Ridge transforms. The complete moment tensor elements are given for earthquakes along the four major transforms in the present study. The magnitudes were adopted from ISC and PDE listings. The moments are in 10^{24} dyn cm. Strike, Dip, Slip of the nodal plane 1 are given References – Dz = Dziewonski *et al.* Papers published in physics of the Earth and Planetary Interior.

Sl. no.	Date D M Y	Time	Latitude	Longitude	Magnitude m_b	Magnitude M_s	Depth km	Seismic moment $M_o \times 10^{24}$ (dyn·cm)	Double Couple ϕ	Double Couple θ	Double Couple λ	M_{11}	M_{22}	M_{33}	M_{12}	M_{13}	M_{23}	Transform name	Ref.
1·	9.8.78	1218:47·3	−20·60	68·68	5·0	4·9	15·0	0·54	149	35	−90								Dz 87b
2·	14.8.78	0323:51·8	−13·89	65·97	4·8	4·8	15·0	1·30	145	67	−170	1·14	−1·16	0·02	−0·31	−0·09	0·62	Argo	Dz 87b
3·	12.10.78	2003:16·3	−8·83	67·28	4·9	5·0	15·0	3·90	229	73	−2	3·80	−3·48	−0·33	−0·53	−0·86	−0·73	Vema	Dz 87b
4.	17.03.79	0632:33·6	−2·84	68·13	5·3	5·3	15·0	3·50											Dz 87c
5.	22.08.79	1224:19·2	−17·44	66·0	5·2	5·2	15·0	10·0	146	70	179	8·70	−7·86	−0·84	−3·61	−2·53	2·40	Marie-Celeste	Dz 87c
6.	14.4.80	1912:04·7	−16·95	66·45	5·6	5·7	15·0	29·0	238	77	9	26·7	−24·1	−2·5	−10·8	−9·4	0·60	Marie-Celeste	Dz 88a
7.	29.11.80	0136:44·6	−17·30	65·46	5·2	4·9	15·0	1·80	56	80	−10	1·69	−1·55	−0·14	−0·74	0·11	0·41	Marie-Celeste	Dz 88a
8.	16.07.81	0911:53·4	−1·41	67·75	4·9	5·1	10·0	2·20											Dz 88b
9.	19.08.81	2250:57·5	−9·32	67·18	5·3	5·8	10·0	21·0	228	85	−5	23·9	−18·1	−5·8	−2·1	−0·10	−1·6	Vema	Dz 88b
10.	7.10.81	1319:25·1	−11·42	66·30	5·9	—	10·0	4·7	356	44	−43	2·89	0·22	−3·11	3·041	0·29	2·0	12°12′S	Dz 88b
11.	7.11.81	0942:59·5	−17·73	66·04	5·6	6·0	10·0	64·0	148	70	−180	57·8	−49·7	−8·1	−27·1	−15·5	16·0	Marie-Celeste	Dz 88b
12.	15.10.82	0258:49·3	−13·82	66·27	5·1	5·2	15·0	2·50	138	87	−178	2·62	−2·37	−0·26	−0·28	−0·03	0·12	Argo	Dz 88c
13.	23.9.83	0918:2·9	−20·51	67·75	5·3	5·3	10·0	3·27											Dz 84
14.	11.6.84	1839:37·1	−13·52	65·80	5·0	5·3	10·0	5·29	144	71	165	4·40	−4·14	−0·26	−1·87	−2·70	0·77	Argo	Dz 85a
15.	17.9.84	0641:52·9	−17·49	65·50	5·4	5·8	10·0	23·9	148	75	173	21·3	−19·0	−2·3	−10·6	−7·0	3·7	Marie-Celeste	Dz 85b
16.	27.10.84	0955:49·3	−11·53	65·76	5·0	5·1	10·0	2·59	231	77	−4	2·77	−2·19	−0·59	−0·51	−0·40	−0·32	12°12′S	Dz 85c
17.	01.12.85	0616:47·2	−16·06	66·53	4·7	4·6	10·0	1·23											Dz 86
18.	21.06.86	2233:22·5	−19·86	66·43	4·6	4·6	15·0	1·60											Dz 87a
19.	20.01.88	2050:55·4	−9·10	67·07	4·8	4·9	15·0	2·20	48	74	−8	2·27	−1·85	−0·42	−0·28	0·31	0·44	Vema	Dz 89a
20.	03.02.88	2025:00·9	−9·06	67·02	5·2	5·1	15·0	4·70	138	86	−176	5·14	−4·23	−0·91	−0·47	0·02	0·30	Vema	Dz 89a

21.	04·05·88	0001:41·0	−17·27	65·91	5·6	—	15·0	9·0	144	72	165	8·18	−7·01	−1·17	−3·30	−5·17	1·27	Marie-Celeste	Dz 89b
22.	27.07.88	1217:10·5	−4·42	67·89	4·8	4·8	15·0	0·76											Dz 89c
23.	11.08.88	1329:30·8	−17·58	65·51	5·6	5·6	15·0	26·0	57	72	−4	24·0	−21·2	−2·8	−10·5	6·2	4·6	Marie-Celeste	Dz 89c
24.	28.04.89	0913:54·8	−20·30	67·12	4·9	4·9	15·0	0·70											Dz 90a
25.	14.05.89	0940:54·7	−13·45	66·06	5·5	5·6	15·0	10·0	142	72	179	9·74	−7·86	−1·88	−2·39	−2·81	1·61	Argo	Dz 90a
26.	12.07.89	0241:38·5	−8·81	67·41	5·1	5·0	15·0	5·40	137	90	180	5·71	−4·98	−0·72	−0·42	—	—	Vema	Dz 90b
27.	07.06.90	0714:51·1	−19·84	66·27	4·8	4·8	15·0	1·20											Dz 91a
28.	08.11.90	1456:08·3	−13·40	66·0	5·0	5·0	15·0	0·72	148	90	−180	0·662	−0·615	−0·047	−0·324	—	—	Argo	Dz 91b
29.	05.11.91	2116:27·1	−17·34	65·70	5·6	6·0	15·0	68·0	150	63	179	55·8	−49·8	−6·0	−30·4	−17·8	24·5	Marie-Celeste	Dz 92

Table 2. Seismic moment release and fraction of seismic slip (slip rate/slip predicted by plate motion) along four major transforms on the Central Indian Ridge. The spreading rates are adopted from NUVEL-1 (DeMets *et al* 1990). Figures in brackets indicate moment release computation based on the global average relation shown in figure 3.

Transform name	Latitude (°S)	Longitude (°E)	Length (km)	No. of events observed $M_s > 6{\cdot}0$	Total moment release $\times 10^{25}$ dyn.cm	Spreading rate(cm/yr)	Seismic slip from above 100°C isotherm (%)	Seismic slip from above 400°C isotherm (%)
Vema	9·0	67·0	300	1	21·82(13·31)	3·6	53(32)	15(9)
12°12'S	12·08	65·35	175	—	3·92(3·19)	3·65	23(18)	5(4)
Argo	14·0	66·00	80	1	12·41(6·92)	3·96	146(90)	30(16)
Marie-Celeste	17·5	66·0	220	9	108·27(57·66)	4·22	398(209)	86(46)

motion taken up seismically. The horizontal components of plate velocities will be obtained for each transform from the observed moment rate tensors. In case of longer transform zones compared to their width, the velocities V_y^y and V_x^y will be of relevance and from (4) the corresponding strain rates will be calculated.

4. Seismicity of the ridge

The earthquakes of magnitude $m_b > 4{\cdot}5$ occurring along the ridge and its vicinity have been compiled from the NOAA epicentral tape, ISS/ISC bulletins and PDE listings during the period 1964–1993. Events prior to 1964 during the period 1912–1963 have been compiled from Gutenberg and Richter (1954) for 1912–1952, and from Rothe (1969) for 1953–1963 and the relocated events during this period have been considered from Stover (1966). A detailed seismicity map showing the locations of earthquakes compiled from various sources listed above for the period 1912–1993 plotted on a bathymetric map as shown in figure 2.

The seismicity and bathymetric pattern of the ridge from equator to 7°S is very complex because of short ridge segments and small offset transforms in this region. Within the precision of epicentral locations, it is very difficult to differentiate the transform events and the axial rift valley events. The tectonics of the ridge in this region is further complicated by the intense seismic activity near Chagos Bank. Between 7°S and 19°S the seismicity correlates well with the NE-SW bathymetric trend of the major transforms offsetting the ridge axis. Four first order transforms offsetting the spreading segments identified on the basis of magnetic anomalies, bathymetry and GLORIA surveys by Fisher *et al* (1971) and Parson *et al* (1993) show a distinct seismicity pattern. These are 'Vema' at 9°S and 67°E, 12°12′S at 12°08′S and 65°35′E, 'Argo' at 14°S and 66°E and 'Marie-Celeste' at 17·5°S and 66°E. South of 19°S the pattern of seismicity is again complicated by several minor ridge axis discontinuities reported by Parson *et al* (1993).

5. Earthquakes along major transforms and moment release pattern

5.1 *Scalar moment release*

The earthquakes correlatable to four major transform faults mentioned above during the period 1912–1993 have been utilized to estimate the cumulative moment release. To establish an empirical relationship between seismic moment and M_s, transform events with CMT solutions for which surface wave magnitude and moment available are utilized. Table 1 contains a list of all such events with details of CMT solutions. It may be pointed out that the magnitudes of events prior to 1964 given by Gutenberg and Richter (1954) and Rothe (1969) are equivalent to 20-s M_s (Geller and Kanamori 1977). The least square relation between the M_s and seismic moment (M_o) established based on 27 transform events belonging to the Central Indian Ridge is shown in figure 3. Also shown is the global average M_s-M_o relationship given by Ekstrom and Dziewonski (1988). It can be seen that the latter relation gives lower moments for a given magnitude than the former. Both the relations have been utilized to convert the magnitudes to moments and the results are compared in table 2. It may be seen that the total moment

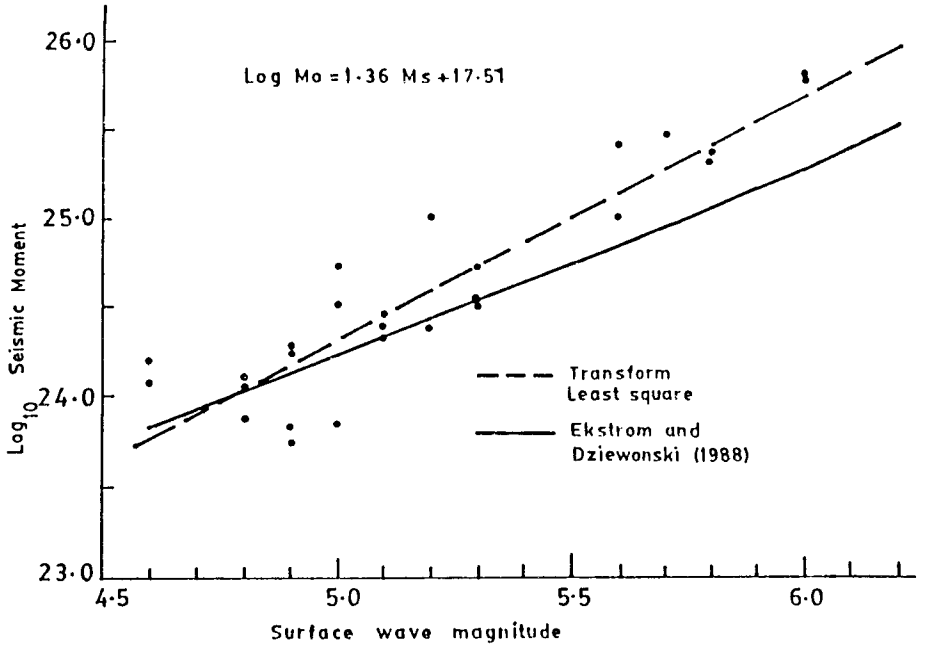

Figure 3. Plot showing the relation between surface wave magnitude and seismic moment for the 27 transform events on the Central Indian Ridge whose moments are known from CMT solutions. The global average relation given by Ekstrom and Dziewonski (1988) is also plotted for comparison.

release and the fraction of seismic slip calculated from the both relationships reveal a similar moment release pattern. The lower values obtained from the global average relation are due to the fact that it is based on earthquakes from widely varying tectonic environments and include many events of $M_s > 6{\cdot}5$. The earthquakes in the present study have mostly $M_s < 6{\cdot}5$. Ekstrom and Dziewonski (1988) identified the Central Indian Ridge as one of the regions in which reported values of M_s are systematically lower, for a given M_o, than the global average. Since the M_s-M_o relations derived from the global data sets or scaling laws underestimate the transform data set as also observed by Engeln *et al* (1986), the transfrom least square relation appears more relevant.

The depth extent of faulting is an important parameter for determining the fractions of seismic and aseismic slip. Assuming the slip is completely seismic, Burr and Solomon (1978) calculated the depth or vertical extent of fault zone (they termed it as fault width) for several transforms worldwide. However, their study was very general and included only earthquakes of $M_s > 6{\cdot}0$ and the depths estimated for the transforms along CIR range from 0·4 to 1·4 km. Using 100°C as the limiting temperature they estimated depths ranging from 0·8–1·3 km. The centroid depths of earthquakes along CIR in the axial region estimated by Huang and Solomon (1987) range from 1·1 to 1·6 km. Since the crust cools while moving away from the axis, brittle failure will extend deeper, and also, as pointed out by Burr and Solomon (1978), the depth of the fault zone increases with increasing length of the transform. As such, the range of vertical extent of fault

zones appear too shallow. Based on the estimate of Engeln *et al* (1986), up to 400°C isotherm for a transform of 12 m.y. age offset, we assumed a value of 5 km as the seismogenic depth. Since the transforms in the present study have less than 12 m.y. offset, the value of 5 km gives a conservative estimate of seismic slip. The total scalar moment release, fractions of seismic slip above 100°C and 400°C isotherms, and slip rates predicted by NUVEL-1 along four transforms are summarized in table 2.

5.2 *Seismic moment rate tensors*

The seismic moment tensors available from the CMT solutions during the period 1977–1993 (Dziewonski *et al* 1984 and subsequent papers in Physics of the Earth and Planetary Interior) are also utilized to study both short (17 years) and long term (82 years) moment release, and to calculate the plate velocities and seismic strain rates along the four transform fault zones by the method detailed in § 3. The moment tensors for twenty earthquakes belonging to four transforms are listed in table 1. For the events for which CMT solutions are not available, their magnitudes were converted to moments using the least square relation shown in figure 3 (as already stated) and the different components of moment tensors were calculated assuming the focal mechanism of the closest CMT event. The length and width of the transform zones were adopted from Fisher *et al* (1971) and Parson *et al* (1993). As mentioned previously, the depth of the seismogenic faulting was assumed as 5 km for all transforms. The transform azimuths and slip vectors were obtained from Fisher *et al* (1971), DeMets *et al* (1990) and Parson *et al* (1993). Almost all slip vectors lie parallel to the strike of the fault zones, except in a few cases where they differ by 2 or 3°. For each transform, the summed moment rate tensor ($\dot{M}$), for the period 1912–1993 and 1977–1993, the matrix **N**, horizontal plate velocities and the corresponding elements of strain tensors are presented in table 3.

6. Tectonic implications

The fractions of seismic slip calculated based on depths of 100°C and 400°C limiting temperature (table 2) reveal that the Marie-Celeste requires a seismic slip almost to a depth of 400°C isotherm to account for the observed moment, while for Argo transform the depth of faulting is much above the 400°C isotherm. The seismic slip rates for Vema and 12°12′S transforms, when compared with the predicted rates, exhibit anomalously low seismic moment release. The style of strain release along the Marie-Celeste is very similar to the Gibbs transform on the Mid-Atlantic Ridge in that, it is characterized by the occurrence of slow events (Okal and Stewart 1982) and the seismic slip mostly accounts for the kinematic slip rate. It is characterized by the presence of positive gravity anomalies in their vicinity (Cochran and Talwani 1977). Further, considering its spatial relation to Reunion hot spot, the asthenospheric pipelines model proposed by Morgan (1978) may have some relevance to account for the seismicity of this transform.

The values of moment rate tensors ($\dot{M}$) for both short and long periods shown in table 3 also reveal anomalously low moment release along Vema and 12°12′S transforms. The higher values of moment rates for 17 years data may be due to short period

Table 3. The components of moment rate tensor, the matrix N, the horizontal plate velocities and the corresponding strain tensors obtained from both short period (1977–1993) and long period (1912–1993) data. Figures in brackets below moment rate components M_{11}, M_{22}, M_{12} are the corresponding $\dot{M}/N$ ratios expressed as percentage. The co-ordinates are $X_1 = E$, $X_2 = N$ and $X_3 =$ up (positive).

Transform name	Dimension (km)	Duration	No. of events	Scalar moment rate $\times 10^{24}$ dyn. cm. yr^{-1}		Moment rate tensor $\times 10^{24}$ dyn. cm. yr^{-1} 11	22	33	12	13	23	Velocities(cm/yr) V_y^y	V_x^y	Strain rates ($\times 10^{-15}$ S^{-1}) ε_y^y	ε_x^y
Vema	l = 300 a = 7 t = 5	1912–1993	39	2·66	$\dot{M}$	0·36	−1·61	1·25	−0·25	0·61	−0·43				
						(2·1)	(9·4)		(5·1)			−0·16	−0·025	−7·33	−0·58
					N	17·1	−17·1		−4·9						
		1977–1993	22	3·15	$\dot{M}$	2·56	−2·39	−0·16	−0·32	−0·21	0·01				
						(14·9)	(13·9)		(6·5)			−0·24	−0·03	−10·8	−0·75
					N	17·1	−17·1		−4·9						
12°12′S	l = 175 a = 7 t = 5	1912–1993	18	0·48	$\dot{M}$	0·09	−0·037	−0·061	−0·039	−0·20	0·02				
						(0·92)	(0·38)		(0·98)			−0·006	−0·006	−0·27	−0·14
					N	9·76	−9·76		−3·94						
		1977–1993	11	1·73	$\dot{M}$	0·40	−0·16	−0·28	−0·05	−0·77	−0·16				
						(4·0)	(1·6)		(1·2)			−0·03	−0·009	−1·22	−0·21
					N	9·76	−9·76		−3·94						
Argo	l = 80 a = 6 t = 5	1912–1993	17	1·51	$\dot{M}$	0·45	−0·345	−0·10	−0·15	−0·28	0·16				
						(9·9)	(7·2)		(7·6)			−0·13	−0·05	−6·87	−1·42
					N	4·56	−4·73		−1·97						
		1977–1993	10	1·39	$\dot{M}$	1·26	−1·21	−0·05	−0·36	−0·40	0·08				
						(27·6)	(25·6)		(18·2)			−0·45	−0·13	−23·7	−3·7
					N	4·56	−4·73		−1·97						
Marie-Celeste	l = 220 a = 15 t = 5	1912–1993	42	13·2	$\dot{M}$	3·89	−4·38	0·484	−4·46	1·707	−0·816				
						(31·8)	(31·8)		(52·2)			−0·60	−0·61	−12·68	−6·85
					N	12·25	−13·78		−8·54						
		1977–1993	23	16·0	$\dot{M}$	13·7	−12·19	−1·52	−5·94	−2·07	3·54				
						(111·8)	(88·4)		(69·5)			−1·67	−0·81	−35·3	−9·1
					N	12·25	−13·78		−8·54						

averaging and it may be recalled that more stable strain estimates can only be obtained by averaging sufficiently longer periods of time intervals (Brune 1968). However, the large discrepancy of values obtained for short and long period data along Marie-Celeste further indicates that this particular transform had large magnitude events with significantly higher moments during 1977–93 (table 1). The estimated strain rates confirm that the transforms have much higher strain rates than the average strain rates for intraplate regions of $10^{-18}\,S^{-1}$ (Wiens and Stein 1983). While highest strain rates were observed along Marie-Celeste transform, the Vema and 12°12′S transforms are characterized by comparatively much lower strain rates. The average strain rates along these two transforms are only slightly higher than the value of $1{\cdot}0 \times 10^{-15}\,S^{-1}$ observed for intense deformation zone in the Central Indian Ocean (Wiens and Stein 1983).

Stewart and Okal (1983) assign the deficiency of seismic moment release to the significant portion of plate motion occurring as aseismic creep. This creep-like behaviour is attributed to the excess magma over a trapped hot spot between the Heezen and Tharp multiple transform fault system (Eltanin system) on the Pacific-Antarctic Ridge. No such excess magmatic activity or presence of a hot spot is reported in the vicinity of the Vema transform. Significantly. along the eastern extension of the Vema transform, the seismicity of Chagos Bank is characterized by the occurrence of several large magnitude earthquakes. The intense intraplate activity near Chagos Bank has been attributed as a part of the diffuse plate boundary in the equatorial Indian Ocean Region (Wiens 1985). The diffuse plate boundary intersects the ridge between 4°N–9°S (Gordon *et al* 1990) and is characterized by abnormally high heat flow anomaly (Stein *et al* 1988). The interaction of this anomalous thermal region with the transform thermal structure would strongly affect the nature of coupling between two walls of the transform fault. This in turn might have influenced the regime of strain release. Though the exact mechanism of interaction is not clear, it is proposed that the deficiency of the moment release along the Vema and 12°12′S multiple transform fault system may be due to most of the plate motion occurring aseismically.

7. Conclusions

We present a detailed seismicity map of the Central Indian Ridge and the events along four major transforms, i.e., the Vema, 12°12′S. Argo and Marie-Celeste were utilized to calculate the moment release pattern. The scalar moment release for the period 1912–1993 and the summed moment rate tensors calculated for both short (1977–1993) and long (1912–1993) periods bring out a unified picture of moment release pattern. While the moment release along the Marie-Celeste and to some extent along Argo transforms are comparable to the seismic slip predicted by plate motion, significant discrepancy between the observed and predicted rates occur along the Vema and 12°12′S transforms giving rise to a very low order of seismic moment release. The calculated strain rates along these two transforms were much lower than the strain rate observed along the Marie-Celeste transform. Along the eastern extent of the Vema transform, the intense Chagos Bank seismicity, a part of the diffuse plate boundary in the equatorial Indian Ocean is characterized by abnormal heat flow anomaly. This, in interaction with the transform thermal structure would strongly affect the nature of coupling between two plates along the transform which in turn would influence the

strain release. The deficiency of moment release along Vema and 12°12'S multiple transform system indicates that a significant portion of the plate motion occurs aseismically.

Acknowledgements

This work was supported by the Department of Science and Technology grant No. SR/OY/A-10/93 under the young scientist scheme. Sincere thanks to Shri T M Mahadevan for his help and many useful suggestions. Critical comments and suggestions made by reviewers were useful in revising the manuscript.

References

Banghar A R and Sykes L R 1969 Focal mechanisms of earthquakes in the Indian Ocean and adjacent regions; *J. Geophys. Res.* **74** 632–649

Brune J N 1968 Seismic moment, seismicity and rate of slip along major fault zones; *J. Geophys. Res.* **73** 777–784

Burr N C and Solomon S C 1978 The relationship of source parameters of oceanic transform earthquakes to plate velocity and transform length; *J. Geophys. Res.* **83** 1193–1205

Cochran J R and Talwani M 1977 Free-air gravity anomalies in the world's oceans and their relationship to residual elevation; *Geophys. J. R. Astr. Soc* **50** 495–552

Davies G F and Brune J N 1971 Regional and global fault slip rates from seismicity; *Nature (London)* **229** 101–107

DeMets C, Gordon R G, Argus D F and Stein S 1990 Current plate motions; *Geophys. J. Inter.* **101** 425–478

Dziewonski A M, Frazen J E and Woodhouse J H 1984 Centroid-moment tensor solutions for July–September 1983; *Phys. Earth Planet. Inter.* **34** 1–8

Ekstrom G and Dziewonski A M 1988 Evidence of bias in estimations of earthquake size; *Nature (London)* **332** 319–323

Ekstrom G and England P 1989 Seismic strain rates in regions of distributed continental deformation; *J. Geophys. Res.* **94** 10,231–10,257

Engeln J F, Wiens D A and Stein S 1986 Mechanisms and depths of atlantic transform earthquakes; *J. Geophys. Res.* **91** 548–577

Fisher R L, Johnson G L and Heezen B C 1967 Mascarene plateau, western Indian Ocean; Geol. Soc. Am. Bull. **78** 1247–1266

Fisher R L, Sclater J G and McKenzie D P 1971 Evolution of the Central Indian Ridge, western Indian Ocean; *Geol. Soc. Am. Bull.* **82** 553–562

Fowler C M R 1990 The solid earth: An introduction to global geophysics (Cambridge: University Press) 471 pp

Geller R J and Kanamori H 1977 Magnitudes of great shallow earthquakes from 1902 to 1952; *Bull Seismol. Soc Am.* **67** 587–598

Gordon R G, DeMets C and Argus D F 1990 Kinematic constraints on distributed lithospheric deformation in the equatorial Indian Ocean from present motion between the Australian and Indian plates. *Tectonics* **9** 409–422

Gutenberg B and Richter C F 1954 *Earthquakes and associated phenomena*, 2nd-ed., (New Jersey: Princeton Univ. Press)

Holt W E, Ni J F, Wallace T C and Haines A J 1991 The active tectonics of the eastern Himalayan syntaxis and surrounding regions; *J. Geophys. Res.* **96** 14, 595–14, 632

Huäng P Y and Solomon S C 1987 Centroid depths and mechanisms of mid-ocean ridge earthquakes in the Indian Ocean, Gulf of Aden, and Red Sea; *J. Geophys. Res.* **92** 1361–1382

Jackson J and McKenzie D P 1988 The relationship between plate motions and seismic moment tensors, and the rates of active deformation in the Mediterranean and Middle East; *Geophys. J.* **93** 45–73

Kanamori, H and Stewart, C S 1976 Mode of the strain release along the Gibbs Fracture Zone, Mid-Atlantic Ridge; *Phys. Earth Planet. Inter.* **11** 312–332

Kostrov V V 1974 Seismic moment and energy of earthquakes and seismic flow of rock; Izv. Acad. Sci. USSR Phys. Solid Earth **1** 23–44

Langseth M G and Taylor P T 1967 Recent heat flow measurements in the Indian Ocean; *J. Geophys. Res.* **72** 6249–6260

McKenzie D P and Sclater J G 1971 The evolution of the Indian Ocean since the late Cretaceous; Geophys. *J. R. Astron. Soc.* **25** 437–528

Morgan W J 1978 Rodriguez, Darwin, Amsterdam.... A second type of hot spot island; *J. Geophys. Res.* **83** 5355–5360

Okal E A and Stewart L M 1982 Slow earthquakes along oceanic fracture zones: Evidence for asthenosphere flow away from hot spots?; *Earth. Planet. Sci. Lett.* **57** 75–87

Parson L M, Patriat P, Searle R C and Briais A R 1993 Segmentation of the Central Indian Ridge between 12°12'S and the Indian Ocean triple Junction; *Mar. Geophys. Res.* **15** 265–282

Rothe J P 1969 *The seismicity of the earth.* UNESCO, Paris pp. 336

Royer J Y, Sclater J G and Sandwell D T 1989 A preliminary tectonic chart of the Indian Ocean; *Proc. Indian. Acad. Sci. Earth Planet. Sci.* **98** 7–24

Sclater J G, Fisher R L, Patriat P, Tapscott C and Parsons B 1981 Eocene to recent development of the Southwest Indian Ridge, a consequence of the evolution of the Indian Ocean triple junction; *Geophys. J. R. Astron. Soc.*, **64** 587–604

Stein C A, Hobart M A and Abbott D H 1988. Has the wharton basin's heat flow been perturbed by the formation of a diffuse plate boundary in the Indian Ocean; *Geophys. Res. Lett.* **15** 455–458

Stewart L M and Okal E A 1983 Seismicity and aseismic slip along the EltaninFracture Zone; *J. Geophys. Res.* **88** 10,495–10,507

Stover C W 1966 Seismicity of the Indian Ocean; *J. Geophys. Res.* **71** 2575–2581

Wald D J and Wallace T C 1986 A seismically active section of the Southwest Indian Ridge; *Geophys. Res. Lett.* **13** 1003–1006

Wiens D A 1985 Historical seismicity near Chagos: A complex deformation Zone in the equatorial Indian Ocean; *Earth Planet. Sci. Lett.* **76** 350–360

Wiens D A and Stein S 1983 Age dependence of oceanic intraplate seismicity and implications for lithospheric evolution; *J. Geophys. Res.* **88** 6455–6468

Wilson J T 1965 A new class of faults and their bearing on continental drift; *Nature (London)* **207** 343–347